

Dear Author,

Please, note that changes made to the HTML content will be added to the article before publication, but are not reflected in this PDF.

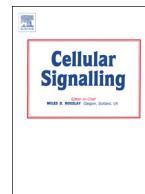
Note also that this file should not be used for submitting corrections.



ELSEVIER

Contents lists available at ScienceDirect

Cellular Signalling

journal homepage: www.elsevier.com/locate/cellsig

Q1 Cell confluence induces switching from proliferation to migratory signaling by site-selective phosphorylation of PDGF receptors on lipid raft platforms

Q2 Árpád Szöör^a, László Ujlaky-Nagy^b, Gábor Tóth^a, János Szöllösi^{a,b}, György Vereb^{a,b,*}

^a Department of Biophysics and Cell Biology, Faculty of Medicine, University of Debrecen, Debrecen, Hungary

^b MTA-DE Cell Biology and Signaling Research Group, Faculty of Medicine, University of Debrecen, Debrecen, Hungary

ARTICLE INFO

Article history:

Received 29 June 2015

Received in revised form 25 November 2015

Accepted 25 November 2015

Available online xxxx

Keywords:

Lipid rafts

Site-selective phosphorylation

Quantitative confocal microscopy

Contact inhibition

Tumor proliferation

Invasive tumor growth

Cell migration

Glioblastoma

PDGFR

ABSTRACT

Platelet derived growth factor receptors (PDGFR) play an important role in tumor pathogenesis and are frequently overexpressed in glioblastoma. Earlier we have shown that only confluent glioblastoma cell cultures exhibit a biphasic calcium transient upon PDGF stimulation. Here, we examined how the change in cell density leads to differential cellular responses to the same PDGF stimulus.

PDGF beta receptors and their specific phosphotyrosine residues were fluorescently co-labeled on A172 and T98G glioblastoma cells. The distribution in cell membrane microdomains (lipid rafts) and the phosphorylation state of PDGFR was measured by confocal microscopy and quantitated by digital image processing. Corresponding bulk data were obtained by Western blotting. Activation of relevant downstream signaling pathways was assessed by immunofluorescence in confocal microscopy and by Western blot analysis. Functional outcomes were confirmed with bulk and single cell proliferation assays and motility measurements.

In non-confluent (sparse) cultures PDGF-BB stimulation significantly increased phosphorylation of tyr716 specific for the Ras/MAPK pathway and tyr751 specific for the phosphoinositide 3-kinase/Akt pathway. As cell monolayers reached confluence, tyr771 and tyr1021 were the prominently phosphorylated residues. Tyr771 serves as adaptor for Ras-GAP, which inactivates the MAPK pathway, and tyr1021 feeds into the phospholipase C-gamma/PKC pathway. Coherent with this, MAPK phosphorylation, Ki67 positivity and proliferation dominated in dispersed cells, and could be abolished with inhibitors of the MAPK pathway. At the same time, RhoA activation, redistribution of cortactin to leading edges, and increased motility were the prominent output features in confluent cultures. Importantly, the stimulus-evoked confluence-specific changes in the phosphorylation of tyrosine residues occurred mainly in GM1-rich lipid microdomains (rafts).

These observations suggest that the same stimulus is able to promote distinctly relevant signaling outputs through a confluence dependent, lipid raft-based regulatory mechanism. In particular, cell division and survival in sparse cultures and inhibition of proliferation and promotion of migration in confluent monolayers. In our model, the ability to switch the final output of the same stimulus as a function of cell density could be a key to the balance of proliferation and invasion in malignant glioblastoma.

© 2015 Published by Elsevier Inc.

1. Introduction

Platelet-derived growth factors (PDGFs) and their receptors (PDGFRs) have been demonstrated as prototypes for growth factor and receptor tyrosine kinase function for more than 30 years. PDGF stimulates migration and proliferation of connective tissue cells and has an important role during embryonic development and wound healing [1], but its abnormal expression also contributes to a variety of diseases [2]. PDGF and its receptor are currently under investigation as targets in numerous proliferative disorders, including cancers, fibrosis, and cardiovascular diseases [2]. PDGFR- β plays an important role in the regulation of human malignant gliomas [3,4]. PDGF and PDGFR expression correlates with tumor grade and proliferative activity [5–7],

Abbreviations: DAG, diacylglycerol; GM1, monosialotetrahexosylganglioside; GRB2, growth factor receptor binding protein-2; IP3, inositol 1,4,5-trisphosphate; PDGF, platelet-derived growth factor; PDGF-BB, homodimer of the B isoform of platelet derived growth factor; PDGFR, platelet-derived growth factor receptor; PI3-kinase, phosphatidylinositol 3'-kinase; PKC, protein kinase C; PLC γ , phospholipase C- γ 1; PtdIns(3,4,5)-P3, phosphatidylinositol (3,4,5)-trisphosphate; PTPN1, protein tyrosine phosphatase, non-receptor, type 1 (PTP1B); Ras-GAP, GTPase activator of Ras; Ras-MAPK, Ras mediated mitogen-activated protein kinase; SH2 domain, Src Homology 2 domain; Tyr716, tyrosine residue 716; Tyr751, tyrosine residue 751; Tyr771, tyrosine residue 771; Tyr1021, tyrosine residue 1021.

* Corresponding author at: Department of Biophysics and Cell Biology, Faculty of Medicine, University of Debrecen, Egyetem tér 1, H-4032 Debrecen, Hungary.

E-mail address: vereb@med.unideb.hu (G. Vereb).

<http://dx.doi.org/10.1016/j.cellsig.2015.11.012>

0898-6568/© 2015 Published by Elsevier Inc.

Please cite this article as: Á. Szöör, et al., Cell confluence induces switching from proliferation to migratory signaling by site-selective phosphorylation of PDGF receptors on..., Cell. Signal. (2015), <http://dx.doi.org/10.1016/j.cellsig.2015.11.012>

and inhibition of PDGFR- β drastically reduces the proliferation and migration of glioblastoma cells [8].

Phosphotyrosine residues on the activated PDGFR initiate downstream signaling. On PDGFR- β , tyrosine 716 (Tyr716) is an important residue which binds the growth factor receptor binding protein-2 (GRB2). This SH2 domain protein activates the Ras-MAPK pathway [9] which plays a central role in cell proliferation. Dephosphorylation of Tyr716 by protein tyrosine phosphatase PTPN1 (PTP1B) inhibits PDGF-induced ERK1/2 MAPK activation [10]. The negative regulation of this pathway is mediated by the phosphorylation of tyrosine 771 (Tyr771) leading to the binding of Ras-GAP, the GTPase activator of Ras [11]. Phosphorylation of Tyr771 is regulated by protein tyrosine phosphatase PTPN11 (SHP-2) [12]. Dephosphorylation of Tyr771 decreases the recruitment of Ras-GAP leading to prolonged activation of the Ras/MAP kinase pathway and thus promoting cell proliferation.

Tyrosine 751 (Tyr751) is situated in the kinase insert region and binds the regulatory p85 subunit of phosphatidylinositol 3'-kinase (PI3-kinase) [13]. The phosphatidylinositol (3,4,5)-trisphosphate (PtdIns(3,4,5)-P₃) generated by PI3-kinase enhances the activity of the pro-survival Akt kinase [14,15]. PTPN1 is also able to dephosphorylate Tyr751 on PDGFR, thus decreasing activation of Akt [10].

Tyrosine 1021 (Tyr1021) is known as the binding site of phospholipase C- γ 1 (PLC γ) [16]. PLC γ initiates the inositol 1,4,5-trisphosphate (Ins (1,4,5)-P₃)/diacylglycerol (DAG) pathway, which mediates intracellular calcium mobilization and protein kinase C (PKC) activation [17] and is important in the regulation of cell migration [16,18].

GM1 rich microdomains (lipid rafts) of the cell membrane play crucial role in growth factor induced signal transduction [19,20]. These plasma membrane microdomains enriched in cholesterol and sphingolipids are able to segregate cellular processes during signal transduction by promoting isolated assembly of membrane protein superstructures [21] and to focus signaling input by accumulation of specific receptors [22,23].

Under normal conditions, cell growth and motility are regulated not only by the availability of growth factors but also by a number of positive and negative co-stimuli delivered by the extracellular matrix and the neighboring cells. Increasing number of cell-cell contacts leads to an arrest of proliferation known as contact inhibition [24]. When normal cells undergo malignant transformation, they can lose contact inhibition causing abnormal cell proliferation and migration [25]. In the case of PDGFR mediated cell proliferation, contact inhibition correlates with low molecular weight phosphotyrosine phosphatase mediated dephosphorylation of the receptor [26].

Previously we have shown that PDGF stimulated glioblastoma cells respond with prolonged biphasic rises of intracellular free calcium concentration when cultures were confluent, however, in sparse cultures this response largely disappears [27]. The distinct behavior was independent of cell cycle [27], however, preliminary experiments hinted that PDGFR expression and lipid raft localization did change with cell culture confluence. Consequently, in the present study we examined how segregation of PDGFR by GM1 rich microdomains could regulate a differential cellular response as a function of cell confluence in glioblastoma cells. We have found that even though the same receptors are stimulated by the same ligand, tyrosine residues that initiate distinct pathways are selectively phosphorylated in lipid rafts and stimulate functions inherently appropriate for the status of tumor cells: sparse cells enter the mitotic cycle, whereas confluent cells start to migrate.

2. Materials and methods

All materials were from Sigma-Aldrich (St. Louis, MO) unless otherwise indicated.

2.1. Cell culture

A172 (CRL-1620) and T98G (CRL-1690) human glioblastoma cells 130 obtained from American Type Culture Collection were maintained in a 131 humidified incubator at 37 °C in a 5% CO₂ atmosphere in Dulbecco's 132 Minimal Essential Medium supplemented with 10% fetal calf serum 133 and antibiotics. Cells were passaged three times a week. 134

For confocal microscopy, cells were seeded onto 12 mm glass coverslips (0.17 mm, Menzel-Glaser, Braunschweig, Germany) at various 135 densities. We used sparse/low density and confluent/high density cell 136 cultures. Initial cell concentration was 15,000/cm² for sparse and 137 60,000/cm² for confluent conditions. Cells were cultured for 2 days 138 before measurements, unless otherwise stated. 139 140

For Western blot experiments, cells were seeded onto cell culture 141 dishes (Corning, via Sigma-Aldrich). Sparse/low density and confluent 142/high density cultures were used. 570,000 cells were seeded in 143 100 mm and 35 mm petri dishes which meant 7250 and 60,000 cells/ 144 cm² for sparse and confluent samples, respectively. Cells were cultured 145 for 2 days before measurements. 146

Before experiments, cells were starved in serum-free HEPES 147 buffer, pH: 7.4, for 2 h at 37 °C. Ligand stimulation of PDGFR- β was 148 done with the recombinant homodimer of the B isoform of platelet 149 derived growth factor (PDGF-BB) at 37 °C. PDGF-BB was used at a 150 final concentration of 20 ng/ml, the lowest dose previously 151 established to cause maximum calcium signals in confluent glioblastoma 152 cell cultures [28]. For microscopy experiments, ligand stimulation 153 was 2 min long when measuring receptor phosphorylation, and 154 2 h when assessing migration and proliferation. In order to 155 determine the time-dependence of the events, PDGF-BB stimulation 156 was performed for 1, 2, 5, 15, 30 and 60 min for Western blot-based 157 analysis of signaling. 158

2.2. Immunofluorescent labeling

Cells on coverslips were washed three times in ice-cold HEPES buffer 160 and incubated with anti-PDGFR- β mAb (10 μ g/ml, RD Systems PR7212) 161 for 10 min on ice. After three washes, Cy3-conjugated secondary goat 162 anti-mouse Fab antibody (Jackson ImmunoResearch Europe Ltd., 163 Suffolk, UK) was added at 15 μ g/ml together with 4 μ g/ml Alexa Fluor 164 488-conjugated cholera toxin B-subunit (Invitrogen/Life Technologies, 165 Carlsbad, CA) for 10 min on ice. The cholera toxin B-subunit binds to 166 monosialotetrahexosylganglioside (GM1) glycosphingolipid rich 167 domains and serves as one of the most widely used markers of lipid 168 rafts. After three washes (1, 3 and 5 min), cells were prefixed with 1% 169 paraformaldehyde for 10 min on ice, then the cell membrane was 170 permeabilized with HEPES buffer containing 0.1% Triton-X 100 and 1% 171 BSA for 10 min. Phosphotyrosine 716, 751, 771 and 1021 residues of 172 PDGFR were labeled with indirect immunofluorescence. Following 173 incubation with the appropriate mAb (sc-16569-R, sc-21902-R, 174 sc-17174-R, sc-12909-R respectively, Santa Cruz Biotechnologies, 175 Dallas, TX, 12 μ g/ml final concentration) for 35 min at RT, cells 176 were washed three times (for 2, 4 and 5 min) with HEPES buffer 177 containing 0.05% Triton-X 100. Primary antibodies were labeled 178 with Alexa Fluor 647 conjugated secondary goat-anti-rabbit 179 antibody (20 min, RT, 10 μ g/ml, Invitrogen/Life Technologies, 180 Carlsbad, CA). After three washes, cells were fixed with 4% freshly 181 depolymerized paraformaldehyde. Finally, the coverslips were 182 mounted with Mowiol. Negative controls with one of the primary 183 antibodies omitted, as well as with single secondary antibodies and 184 with no labeling at all were also prepared and confirmed to lack signal 185 in the appropriate fluorescence channel. 186

For microscopic assessment of cell proliferation and cell migration, 187 intracellular indirect labeling was performed using the same protocol 188 as above, starting with washing, fixation and permeabilization. Primary 189 antibodies were used at 4 μ g/ml (M7240 against Ki67 from Dako, 190 Glostrup, Denmark, and 05-180 antibody against cortactin from Merck 191

192 Millipore, Darmstadt, Germany) or at 8 $\mu\text{g}/\text{ml}$ (sc-32,954 against
193 p(Ser188)RhoA from Santa Cruz Biotechnologies, Dallas, TX). Secondary
194 goat anti-mouse (against M7240 and 05–180) and goat anti-rabbit
195 (against sc-32,954) antibodies from Invitrogen/Life Technologies were
196 either Alexa Fluor 647 or Alexa Fluor 546 conjugated and used at
197 10 $\mu\text{g}/\text{ml}$ final concentration.

2.3. Confocal laser scanning microscopy

198

Membrane distribution of PDGFR- β and its phosphotyrosine 199
residues was quantitatively analyzed by a confocal laser scanning 200
microscope (LSM 510, Carl Zeiss GmbH, Jena, Germany). Alexa Fluor 201
488 was excited at 488 nm, Cy3 and Alexa Fluor 546 at 543 nm, and 202

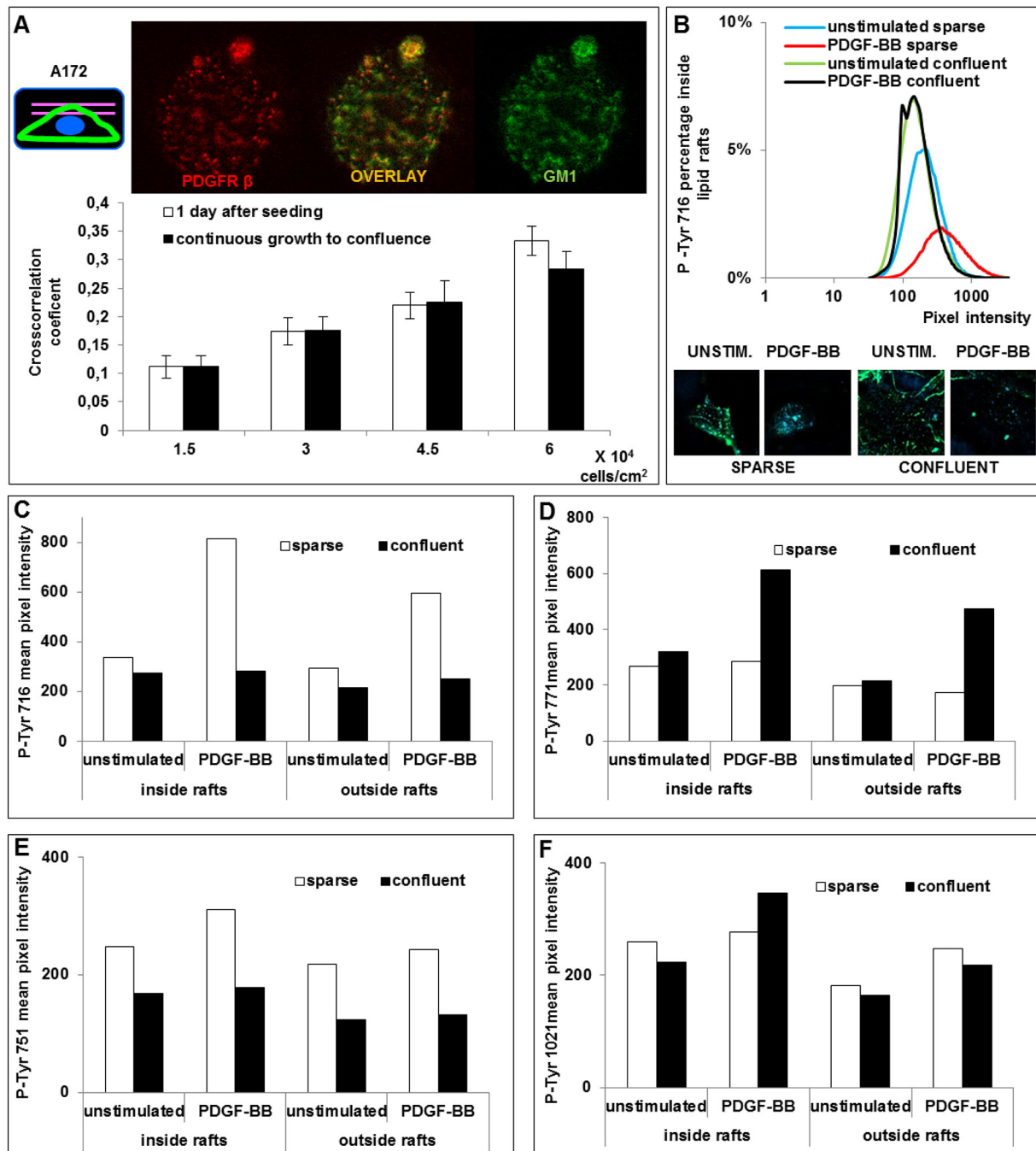


Fig. 1. Residue-specific phosphorylation of PDGFR- β is confluence and lipid raft dependent. **A:** Raft localization of PDGFR receptors as a function of cell confluence. Schematic drawing on the left indicates the position of confocal slice in the cell used for analysis. Images (from a $14.6 \times 14.6 \mu\text{m}^2$ area) show localization and visual colocalization of PDGFR receptors (red) and GM1-rich lipid rafts (green) in A172 cells. Cross-correlation coefficients in the graph below indicate the extent of colocalization as a function of cell density. Data are averages of the cross-correlation coefficient \pm SEM of 40–60 cells from 3 independent experiments. **B:** Quantitation of specific tyrosine phosphorylation in microscopic images. For an example, pixel-by-pixel intensity distribution of p-Tyr716 inside lipid rafts is shown here as a function of cell confluence and PDGF-BB stimulus. The confocal images ($21.3 \times 21.3 \mu\text{m}^2$) show lipid rafts in green, and p-Tyr716 in blue. **C; D; E and F:** Specific tyrosine phosphorylation as function of cell confluence and PDGF-BB stimulus. Mean pixel intensities before and after 20 ng/ml PDGF-BB stimulation are derived from the intensity distribution curves exemplified in **B**. Sparse (open columns) and confluent (filled columns) cultures were of densities 2×10^4 cells/cm² and 1×10^5 cells/cm². p-Tyr716 (**C**), p-Tyr771 (**D**), p-Tyr751 (**E**) and p-Tyr1021 (**F**) were quantitated both inside and outside lipid rafts. (For interpretation of the references to color in this figure legend, the reader is referred to the web version of this article.)

Alexa Fluor 647 at 633 nm. Their fluorescence emission was detected through 505 to 550-nm, 560 to 615 band-pass and 650-nm long-pass filters, respectively. The images were taken in multitrack mode to completely exclude channel cross talk. 512 × 512-pixel, 1.5 μm thick optical sections were obtained with a 40× C-Apochromat water immersion objective (NA = 1.2).

2.4. Determining colocalization from image cross-correlation

Colocalization of any two molecules at the few-hundred-nanometer scale was determined from confocal laser scanning microscopy images of double-labeled cells. The optical section was taken from the top horizontal slice of the membrane of adherent cells (Fig. 1A). The images were gated on the presence (above-background intensity) of at least one of the fluorophores. For a pair of images, x and y, the cross-correlation coefficient C of the two labels was calculated as:

$$C = \frac{\sum_i \sum_j (x_{i,j} - \bar{x})(y_{i,j} - \bar{y})}{\sqrt{\sum_i \sum_j (x_{i,j} - \bar{x})^2 \sum_i \sum_j (y_{i,j} - \bar{y})^2}}$$

where x_{ij} and y_{ij} are fluorescence intensities at pixel coordinates i, j in images x and y and \bar{x} and \bar{y} designate the mean intensities in each channel. The theoretical maximum is $C = 1$ for identical images and a value close to 0 implies independent random localization of the labeled molecules. A custom program written in LabView was used to analyze the images [23]. The average intensity of labels in the membrane was also evaluated by the program.

2.5. Digital image processing for quantitative analysis of specific phosphotyrosine distribution inside and outside of lipid rafts

A quantitative digital image processing pipeline, created for this purpose in ImageJ [29], was used to calculate specific phosphotyrosine density inside and outside of lipid rafts. First, background intensities of phosphotyrosine and GM1 positive channels were subtracted. Two binary masks in inverse relation – raft and non-raft – were created and used to generate inside raft and outside raft phosphotyrosine images. From these, probability distribution curves of pixel-intensities were generated, and the mean intensities calculated (see Fig. 1B–F).

2.6. Digital image processing for quantitative analysis of specific relative receptor phosphorylation inside and outside of lipid rafts

The ImageJ algorithm developed for this purpose starts by subtracting the background in the PDGFR, phosphotyrosine and GM1 channels, and then normalizes the intensity of the specific phosphotyrosine label to the total PDGFR on a pixel by pixel basis. The image generated this way represents the relative specific PDGFR phosphorylation on the cell surface. Raft and non-raft binary mask are then created from the GM1 channel and applied to calculate the mean relative receptor phosphorylation inside and outside of lipid rafts. Finally, the inside raft value is normalized to the outside raft value, so that acquisition parameters that could change across experiments are canceled and allow the pooled evaluation of results from many independent experiments (Fig. 2A). Values of the final quotient above and below 1 indicate preferential phosphorylation and dephosphorylation, respectively, of a given tyrosine residue inside rafts (Fig. 2C–F).

2.7. Western blotting

Cells were washed with ice cold HEPES buffer and lysed with RD lysis buffer containing 20 mM of Tris, 0.1% NP40, 137 mM of NaCl, 10% glycerol, 2 mM of EDTA, 2 mM of PMSF, 1 mM of Na-ortho-vanadate, and Protease Inhibitory Cocktail, (ROCHE, according to

the manufacturer's instructions). Protein concentration was measured according to Bradford, samples were diluted with SDS-PAGE sample buffer to contain the same concentration of total protein and finally boiled for 10 min. Proteins (20 μg per well) were separated by 6–12% SDS-PAGE gels depending on the targeted molar mass, and electrophoretically transferred to polyvinylidene difluoride membranes (Merck Millipore, Darmstadt, Germany). The same antibodies against phosphotyrosine-residues 716, 751, 771, 1021, and pRhoA as for microscopy were used at 0.5 μg/ml. pP38 MAP kinase, pP42/44 MAP kinase, and pAkt were detected with the following antibodies: 9211S (0.3 μg/ml, Cell Signaling Technology, Danvers, MA), 9106S (0.3 μg/ml, Cell Signaling), and 05–669 (0.7 μg/ml, Merck Millipore, Darmstadt, Germany). Total cellular protein was controlled by detecting actin with antibody A3853 (0.1 μg/ml, Sigma-Aldrich, St. Louis, MO). After overnight incubation on a rocking table at 4 °C, membranes were washed with TBS-T (50 mM Tris, 150 mM NaCl, 0.1% Tween 20) for 30 min at room temperature, then peroxidase-conjugated secondary goat anti-mouse (A4416) or goat anti-rabbit (A0545) antibody (1 μg/ml, Sigma-Aldrich, St. Louis, MO) was added for 2 h. After a 30-min wash with TBS-T, membranes were developed with Super Signal West Pico Chemiluminescent Substrate (Thermo Fischer Scientific, Waltham, MA) for 2 min and imaged with a FluorChem Q system (ProteinSimple, San Jose, CA).

2.8. Assessment of cell proliferation

Proliferation in confluent and sparse cultures was measured using an MTT based colorimetric assay (EZ4U, Biomedica GmbH, Wien, Austria). Cells plated at various densities (9000 through 150,000/cm²) were grown in 96-well plates for 2 days. After incubation with EZ4U, a Synergy HT Multi-Detection microplate Reader (Bio-Tek, Winooski, VT) was used to measure 488 nm absorption, which was corrected with the 620 nm absorption and then converted to cell numbers using a calibration curve prepared using parallel measurements of freshly plated and adhered cells seeded at various densities. Cell numbers were averaged (n = 6), and growth was expressed as a multiple of initial cell number, and plotted as a function of initial cell density.

To follow the growth rate continuously, real time cell adherence assay (RTCA) based on impedance measurement was performed using an ECIS Z0 analyzer (Applied Biophysics, Troy, NY). T98G cells were grown in 8W10E PET 8-well arrays with gold electrodes at the bottom, seeded at low (15,000/cm²) and high (60,000/cm²) densities. Weak alternating current was applied at frequencies from 1 to 100,000 Hz to continuously measure the complex impedance spectrum of cells adhering to each electrode in the well. The measured impedance at any time point is proportional to the area of the electrode covered by cells. Impedance values from 4 wells were averaged, normalized to initial cell number, and plotted as a function of time.

For testing the antiproliferative effect of various MAPK pathway inhibitors, we have used live cell imaging followed by cell counting, so that mitotic events could be visually verified. This way the possible metabolic effects of the inhibitors influencing the MTT-based colorimetric assays could be avoided. Cells were seeded at 8000/well into 96-well plates, and allowed to adhere and spread for 20 h in complete medium (with 10% FCS) in a CO₂ incubator. Consecutively, cells were washed, the medium was exchanged for DMEM with 2% FCS and 2 ng/ml of PDGF-BB, various inhibitors were added as needed, and the plate was transferred to a 37 °C, 5% CO₂ chamber on an Olympus IX81 inverted microscope. Time-lapse imaging was performed, taking one frame at every 10 min using an Olympus xcellence^{RT} system. Cells were counted at start and at 24 h using the cell counter module of ImageJ [29]. Cell growth in 24 h was expressed as multiple of initial cell numbers and plotted as mean ± SD (n = 3). Inhibitors against the p38 MAPK, p42/44 MAPK, Erk5 and JNK kinase pathways were from Medchem Express Europe (Stockholm, Sweden) and used at their published biological IC₅₀ concentrations as follows. SB203580 against p38 MAPK (15 μM), U0126

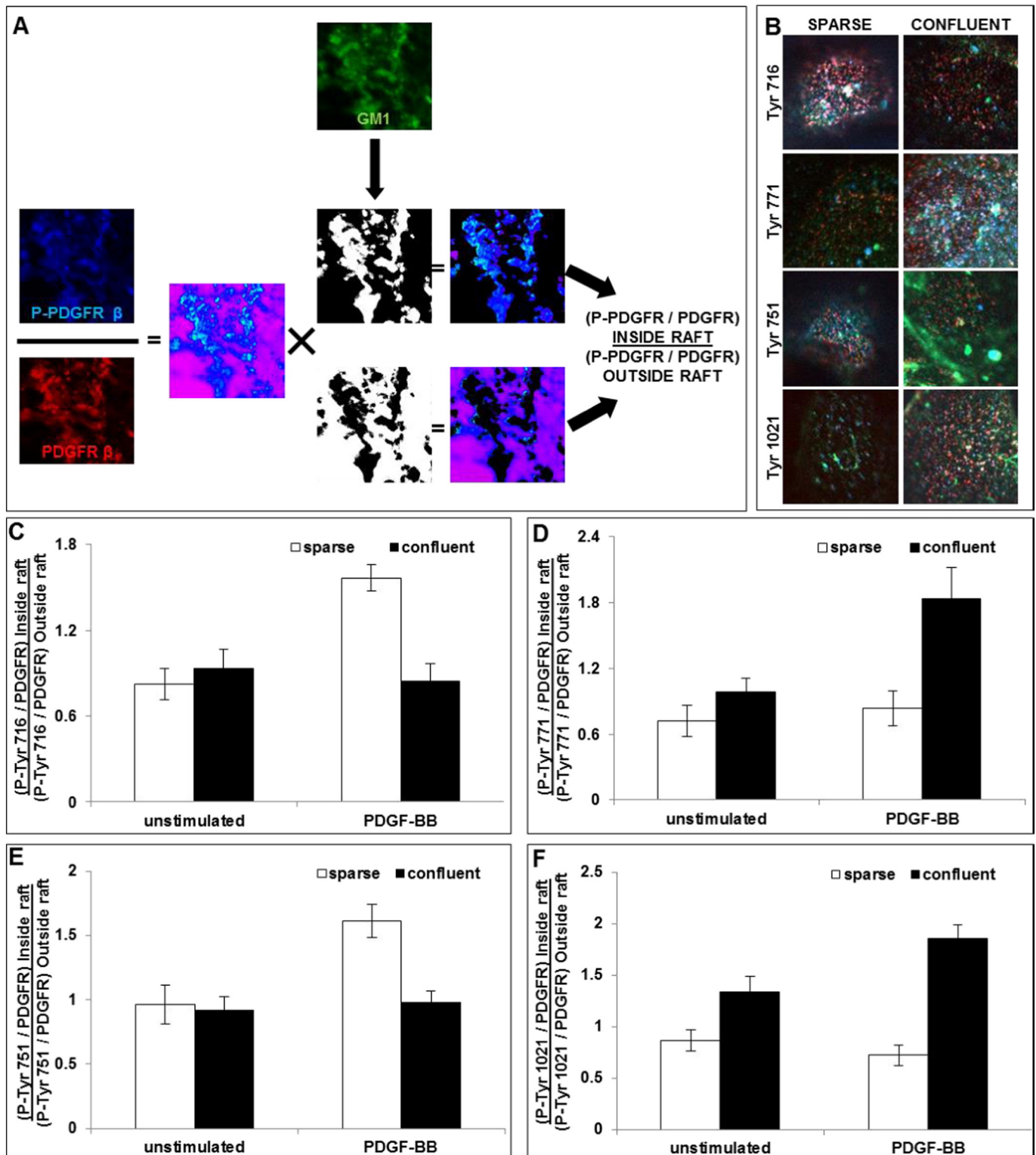


Fig. 2. Quantitative analysis of relative specific receptor phosphorylation in membrane microdomains A: Digital image processing algorithm for quantitative characterization of relative specific receptor phosphorylation in the cell membrane. An example is shown for labeling total (red) and tyrosine phosphorylated (blue) receptors as well as lipid rafts (green), and using the lipid raft image as a binary mask for deriving an numeric characterizing raft vs. non-raft based relative phosphorylation status independent of labeling and detection efficiency. B: Confocal images provide information about the membrane distribution of cell surface receptors (red), specific phosphotyrosine residues (blue) and lipid rafts (green). The images ($21.3 \times 21.3 \mu\text{m}^2$) taken after 2 min stimulation with 20 ng/ml PDGF-BB show that in A172 glioblastoma PDGFR, p-Tyr716 and p-Tyr751 colocalize with GM1 rich domains of the sparse cultures, while p-Tyr771 and p-Tyr1021 are more abundant in rafts of confluent cultures, as indicated by stronger intensities and more white spots where the three label colors colocalize. C, D; E and F: Ratio of raft and non-raft specific relative receptor tyrosine phosphorylation. Sparse (open columns) and confluent (filled columns) cultures were of densities 2×10^4 cells/cm² and 1×10^5 cells/cm², respectively. p-Tyr716 (C), p-Tyr771 (D), p-Tyr751 (E) and p-Tyr1021 (F) were quantitated before and 2 min after stimulation with 20 ng/ml PDGF-BB. Data are averages of the ratios \pm SEM of 40–60 cells from 3 independent experiments. (For interpretation of the references to color in this figure legend, the reader is referred to the web version of this article.)

320 against MEK1/2 phosphorylating p42/44 MAPK (Erk1/2) (5 μ M),
 321 BIX02188 against MEK 5 phosphorylating Erk5 (1 μ M), SP600125
 322 against JNK1,2,3 (10 μ M), and Kobe0065 inhibiting activation of Raf by
 323 Ras (10 μ M).

324 2.9. Measurement of cell motility

325 In order to measure cell motility, we used the Olympus xcellence^{RT}
 326 live cell imaging system with a 37 °C, 5% CO₂ chamber on an Olympus
 327 IX81 inverted microscope. Cells were seeded in complete medium at
 328 8000 and 32,000 per well in 96-well plates and allowed to adhere for
 329 20 h. The medium was exchanged for DMEM with 2% FCS and 2 ng/ml
 330 PDGF-BB, and cells were imaged at every 10 min for a minimum of
 331 36 h using a 10 \times objective with 645 nm/pixel resolution. The MTrackJ
 332 plugin [30] of ImageJ was used to track individual cells. The center of
 333 mass for each cell was tracked until the first mitotic event [31,32].
 334 Track data from three experiments (n \geq 100 for each condition) were
 335 exported and analyzed with the Chemotaxis and Migration Tool
 336 (v.2.0) from ibidi GmbH (Martinsried, Germany). The analyzed time
 337 span was increased from 100 min to 1500 min in 100 min steps to be
 338 able to account for the various times taken by each cell before mitosis
 339 (all observed cells divided before 1500 min). Accumulated distance
 340 and Euclidean distance (absolute displacement) were plotted as a func-
 341 tion of observation time. Average velocity of cells did not change much
 342 with the length of observation time, and therefore the average velocities
 343 derived from the full length tracks were plotted. Graphs representing all
 344 cell tracks centered to start at coordinates (0,0) were plotted for 200,
 345 500 and 1500 min observation time and overlaid for sparse and conflu-
 346 ent cultures.

347 3. Results

348 3.1. Lipid raft localization of PDGFR- β in the cell membrane is a function of 349 cell culture confluence

350 Preliminary experiments have shown that expression of PDGFR- β in
 351 A172 glioblastoma cells increases with confluence of cells in culture and
 352 that these receptors are mainly localized to GM1 rich lipid microdo-
 353 mains also termed lipid rafts. To quantitate the degree of overlap
 354 between clusters of PDGFR- β and submicron sized lipid rafts, we
 355 employed confocal microscopy yielding 1.5 μ m thick optical slices of
 356 the upper cell membrane. Colocalization was quantified by calculating
 357 the cross correlation coefficient. Overlap of PDGFR with lipid rafts was
 358 directly proportional to the confluence of the monolayer, regardless of
 359 whether cells were seeded at varying densities and measured after
 360 having adhered to the substrate, or seeded at the same density, and
 361 left to grow continuously over several days to reach increasing levels
 362 of confluence (Fig. 1A). This indicated that cell culture confluence as a
 363 state and not the process of reaching it regulates receptor expression
 364 and raft localization.

365 3.2. Phosphorylation of specific residues on PDGFR- β also depends on cell 366 confluence and is a function of raft localization

367 To investigate whether the confluence dependent raft localization of
 368 the receptors has any functional consequence, we quantitated the
 369 amount of specific phosphotyrosine residues inside and outside GM1
 370 rich membrane domains both in resting and PDGF-BB stimulated cells
 371 by immunofluorescence. We calculated the pixel by pixel distribution
 372 of specific phosphotyrosine residues both inside and outside lipid
 373 rafts. An example is shown in Fig. 1B for the case of p-Tyr716 localized
 374 inside rafts. Here, sparse cultures exhibited basal phosphorylation of
 375 Tyr716 inside rafts slightly higher than confluent cultures, and showed
 376 a greatly increased activation upon stimulation with PDGF-BB, whereas
 377 the confluent cultures hardly increased p-Tyr716 in their rafts upon
 378 stimulus. Overall, we found that the mean of the log-normal

distributions serves well to characterize the specific activation of the
 tyrosine residues of interest, namely that of Tyr716, Tyr751, Tyr771
 and Tyr1021.

The means of histograms revealed a raft-dependent inverse pattern
 of activation of residues Tyr716 and Tyr771, which oppositely regulate
 the Ras-MAPK pathway, as a function of cell culture confluence. Follow-
 ing PDGF-BB stimulation, Tyr716 residues, responsible for activating the
 Ras-MAPK pathway, were mainly phosphorylated in sparse cultures,
 and a greater part of them in GM1 rich domains (Fig. 1C). Tyr771 on
 the other hand, which negatively regulates the Ras-MAPK pathway
 through activating Ras-GAP, was more phosphorylated in confluent
 cultures, but also with a dominance of lipid raft-localized receptors
 (Fig. 1D). Cell confluence had no prominent effect on the baseline
 activation of Tyr716 and Tyr771; overall, sparse cultures exhibited
 1.3 \times and 0.9 \times the phosphorylation for these residues compared to
 confluent ones.

Basal phosphorylation of Tyr751 responsible for activating the
 PI3K-Akt pathway was 1.6 \times higher in sparse than in confluent cultures.
 Following PDGF-BB stimulus, sparse cells showed increased phosphory-
 lation inside lipid rafts (Fig. 1E). Tyr1021 phosphorylation, which
 triggers calcium response by activating PLC γ , was globally higher in
 GM1 rich membrane areas, and exhibited considerable increase upon
 ligand stimulation in confluent cells (Fig. 1F).

The differences seen so far represent absolute p-Tyr levels in the
 vicinity of the membrane. However, to properly assess the role of lipid
 rafts in segregating phosphorylation-dephosphorylation processes, we
 must also consider the trends in relative specific receptor phosphoryla-
 tion. The image processing algorithm is depicted in Fig. 2A. First, specific
 phosphotyrosine signal intensities were normalized pixel by pixel to the
 total PDGFR signal to obtain relative PDGFR phosphorylation in the cell
 membrane. Next, the binary mask created from thresholding the GM1
 signal was used to generate the ratio of relative phosphorylation inside
 and outside GM1 rich domains. The added benefit of this approach is
 that differences in labeling intensities across independent experiments
 are equalized and thus several independent experiments can be cumu-
 lated (Fig. 2A).

Fig. 2B shows examples of triple labeling the PDGFR, one of its specif-
 ic p-Tyr residues, and GM1 gangliosides. Processing these images using
 the double normalization approach (Fig. 2A) highlights the role of lipid
 rafts in executing specific phosphorylation: upon PDGF stimulation, the
 specific phosphorylation of PDGFR normalized to total PDGFR was al-
 ways higher inside rafts than outside rafts. This increase was restricted
 by the state of confluence and the tyrosine residue of interest. Residue
 Tyr716 (Fig. 2C) activating the Ras-MAPK pathway was prominently
 phosphorylated in sparse cells, whereas Tyr771 (Fig. 2D) inhibiting
 the same pathway was phosphorylated in confluent cells. Tyr751 (Fig.
 2E), stimulating the Akt kinase, showed increased relative phosphoryla-
 tion in sparse cells. However, relative activation of Tyr1021, the docking
 site for PLC γ , was significantly higher in rafts of confluent cells (Fig. 2F).
 These observations correlate well with data on absolute phosphoryla-
 tion levels in Fig. 1, and corroborate the idea that cell confluence influ-
 ences the morphological segregation in lipid rafts and differential
 phosphorylation on specific tyrosine residues of PDGF receptors and
 thereby induces alternative cellular functions.

379 3.3. Activation of the ras-MAPK pathway and consequential cell prolifera- 380 tion is dominant in sparse cultures

381 We performed Western blot analysis to confirm that the selective
 382 tyrosine phosphorylation depends on cell confluence and to test the
 383 activation of relevant downstream signaling pathways. To reveal
 384 whether the findings can be generalized, a second PDGFR expressing
 385 glioblastoma cell line, T98G, was also examined in addition to A172
 386 cells.

In accordance with microscopy data, levels of p-Tyr716 which
 activates the Ras-MAPK pathway showed a transient increase in sparse

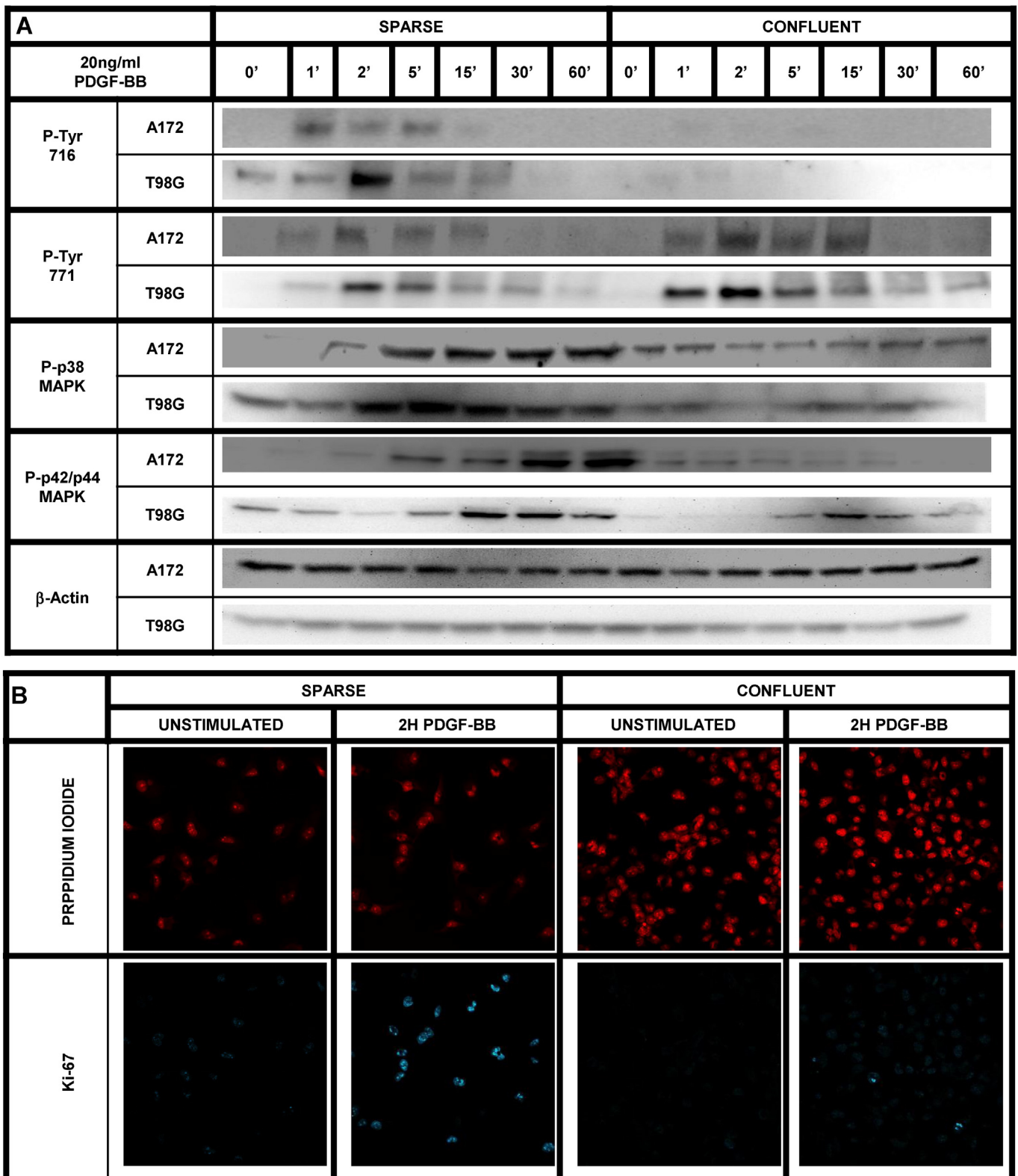


Fig. 3. Proliferative signal routes are boosted in sparse and suppressed in confluent cultures A: Western blot analysis of various phosphorylated proteins involved in MAPK signaling as a function of post-stimulus time. Following 0, 1, 2, 5, 15, 30 and 60 min stimulation with 20 ng/ml PDGF-BB, phosphorylated Tyr716, Tyr771, p38 and p42/p44 MAPK were probed in sparse (1×10^4 cells/cm²) and confluent (1×10^5 cells/cm²) A172 and T98G glioblastoma cell cultures. Anti-β-actin antibody was used as loading control in addition to equalizing total protein in the samples. B: Quantitation of proliferation induced by PDGF-BB treatment. Immunofluorescent analysis of Ki-67 (blue) shows proliferating cells in sparse (2×10^4 cells/cm²) and confluent (1×10^5 cells/cm²) A172 glioblastoma cultures. Propidium iodide was used to visualize all nuclei of the microscopic field (red). The images ($117 \times 117 \mu\text{m}^2$) taken after a 2-h stimulation with 20 ng/ml PDGF-BB show that Ki-67 activation increased in the nuclear region of ~85% of the cells in sparse cultures. (For interpretation of the references to color in this figure legend, the reader is referred to the web version of this article.)

443 cultures of both cell lines following PDGF-BB ligand stimulation, and no
 444 change in confluent cells. Conversely, increased phosphorylation of the
 445 Tyr771 residue activating Ras-GAP, an inhibitor of the pathway, was
 446 more prominent in confluent cultures, although some transient
 447 phosphorylation was also seen in sparse cultures. Next, we measured
 448 the phosphorylation of two effector MAPK isoforms, p38 MAPK, and
 449 p42/p44 MAPK. Coherent with the specific phosphorylation of tyrosine
 450 residues activating and inhibiting these MAP kinases, both p38 and p42/
 451 p44 were activated mainly in sparse cultures. We have observed a time
 452 delay between the activation of receptors and effector proteins: while
 453 Tyr 716 and Tyr 771 residues were maximally phosphorylated within
 454 1–2 min of ligand stimulus, and by 15 min were already back to
 455 baseline; activation of effector MAP kinases peaked in the range of
 456 5–30 min, and lasted through the 60 min observation period (Fig. 3A).

457 Since activation of the MAP kinase pathway is expected to influence
 458 cell proliferation; accumulation of the Ki-67 proliferation marker in cell
 459 nuclei was also assessed by fluorescence microscopy. In line with in-
 460 creased MAPK activation in sparse cultures, we found greatly increased
 461 Ki-67 protein levels in the nuclear region of ~85% of the cells in sparse
 462 cultures 2 h after PDGF stimulus. Coherent with low MAPK activation,
 463 the proportion of highly Ki-67 positive cells was only 1% in confluent
 464 cultures, and a further 12% exhibited a slight increase. Without stimulus,
 465 no signs of proliferation were detected in either state of the serum
 466 starved cell cultures (Fig. 3B).

467 We have used an MTT based assay to show direct evidence of
 468 increased proliferation in sparse cultures. Both A172 and T98G cells
 469 were seeded at densities in the range of 9000/cm² to 150,000/cm²
 470 and final cell number normalized to initial cell number was plotted
 471 as a function of seeding density. As evident from Fig. 4A, the lowest
 472 density cultures of both A172 and T98G nearly doubled in two
 473 days, proliferation gradually dropped with increasing initial cell
 474 numbers, and cell cultures with very high seeding density did not
 475 grow in terms of metabolic activity, or even showed decreased MTT
 476 oxidation.

477 We also showed how the time course of proliferation rates differ for
 478 the confluent and sparse cultures of T98G cells using impedance based
 479 real time cell adhesion (RTCA) measurements. Fig. 4B shows the
 480 increasing surface coverage of these cells as a function of time. During
 481 the first 20 h, as confirmed by live cell microscopy, the cells first attach,
 482 and then start spreading on the substrate (marked by the black arrow).
 483 Once spreading is finished (dashed arrow), they start proliferation. The
 484 rate of proliferation (the slope of surface coverage normalized to initial
 485 cell number vs. time) is much greater for sparse cultures. One should
 486 note that without normalization to initial cell number (a factor of 4
 487 between spares and confluent cells), the impedance is of course higher
 488 for confluent cultures, but the relation of slopes remains the same. In
 489 addition confluent cultures saturate the well sooner and no further
 490 increase of impedance can be detected.

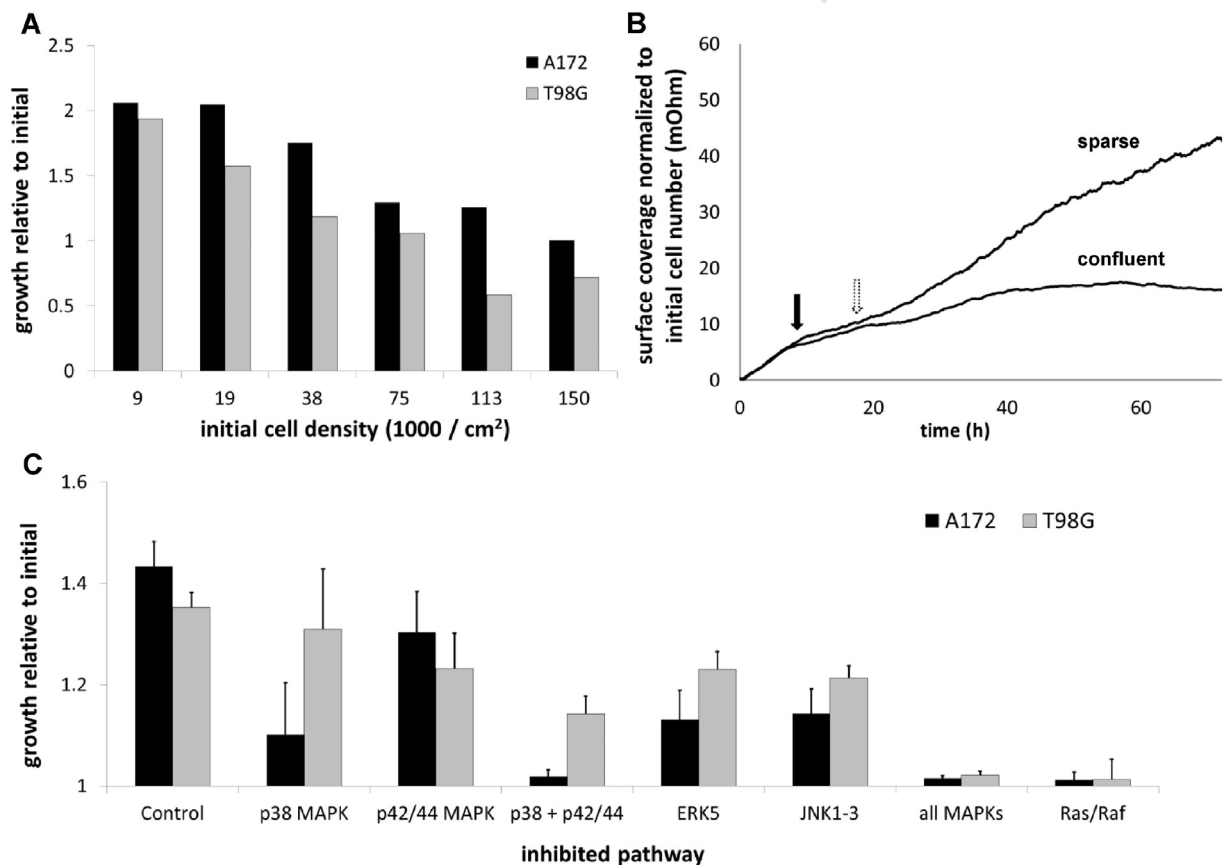


Fig. 4. Cellular outcome of increased proliferative signaling in sparse cultures and its dependence on various MAP kinase pathways A: Cell proliferation as a function of cell density Cells plated at various densities (9000 through 150,000/cm²) were grown in 96-well plates for 2 days. Readout of the MTT-based assay was calibrated to know numbers of freshly adhered viable cells of the same type, averaged for 6 measurements, normalized to the initially seeded cell number and plotted as its function. B: Real time cell proliferation as a function of cell density Real time cell adherence assay (RTCA) was done on T98G cells seeded to be sparse (15,000/cm²) or confluent (60,000/cm²) using an ECIS Z θ analyzer. The measured impedance at any time point is proportional to the area of the electrode covered by cells. Impedance values from 4 wells were averaged, normalized to initial cell number, and plotted as a function of time. Black arrow: end of attachment phase, dashed arrow: end of spreading on substrate and beginning of proliferation. C: Effect of inhibiting MAPK pathways on cell proliferation Cells were seeded at 8000/well into 96-well plates, allowed to adhere and spread for 20 h then stimulated with 2 ng/ml PDGF-BB in the absence or presence of various specific inhibitors: SB203580 against p38 MAPK (15 μ M), U0126 against MEK1/2 phosphorylating p42/44 MAPK (5 μ M), BIX02188 against MEK 5 phosphorylating Erk5 (1 μ M), SP600125 against JNK1,2,3 (10 μ M), and Kobo0065 inhibiting activation of Raf by Ras (10 μ M). Cells were imaged using an Olympus xcellence^{RT} system for 24 h and cell growth was expressed as multiple of initial cell numbers and plotted as mean \pm SD (n = 3).

491 3.4. Multiple MAP kinases are responsible for the proliferation

492 To show the contribution of the various MAPKs to cell proliferation,
 493 we applied specific inhibitors of the p38 MAPK, p42/44 MAPK, Erk5 and
 494 JNK pathways (Fig. 4C). We found that in A172 cells inhibition of p38
 495 MAPK with the published biological EC50 dose of SB203580 decreased
 496 the proliferation by ~75%, while inhibiting the p42/44 MAPK pathway

through MEK1/2 by U0126 caused only ~30% decrease. Combination
 of the two inhibitors, however, caused nearly complete inhibition.
 T98G cells behaved differently, and inhibition of p38 and p42/44
 MAPK pathways resulted in only ~10% and ~35% decrease of prolifera-
 tion, and their combination appeared additive. Consequently, we have
 also tested BIX02188 to inhibit Erk5 via MEK5, SP600125 to inhibit the
 JNK kinases, and Kobe0065 to inhibit the Ras/Raf interaction which

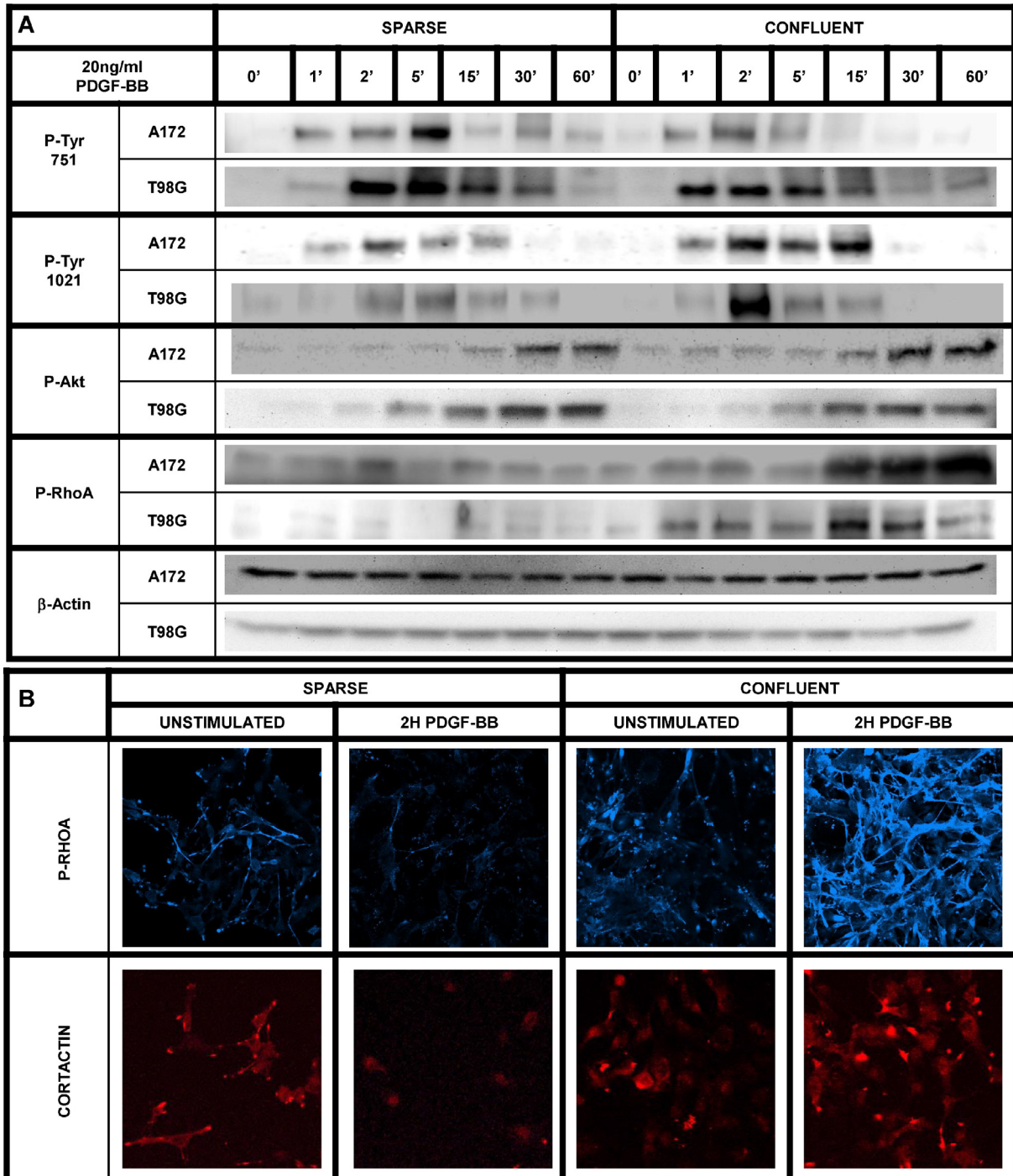


Fig. 5. Confluent, but not sparse, cell cultures exhibit molecular signs of stimulus induced migratory response A: Western blot analysis of various phosphorylated proteins involved in PI3-K and PLC γ signaling as a function of post-stimulus time. Following 0, 1, 2, 5, 15, 30 and 60 min stimulation with 20 ng/ml PDGF-BB, phosphorylated Tyr751, Tyr1021, Akt and RhoA were probed in sparse (1×10^4 cells/cm 2) and confluent (1×10^5 cells/cm 2) A172 and T98G glioblastoma cell cultures. Anti- β -actin antibody was used as loading control in addition to equalizing total protein in the samples. B: Visualization of proteins involved in cell migration after PDGF-BB treatment. Immunofluorescent labeling of phospho-RhoA (blue) and cortactin (red) in sparse (2×10^4 cells/cm 2) and confluent (1×10^5 cells/cm 2) A172 glioblastoma cell cultures before, and 2 h after 20 ng/ml PDGF-BB stimulus shows increased migratory signaling in confluent, and decreased signaling in sparse cultures after PDGFR activation. Images are from $87.6 \times 87.6 \mu\text{m}^2$ fields of view. (For interpretation of the references to color in this figure legend, the reader is referred to the web version of this article.)

can serve as a starting point of these cascades, when activated by the phosphorylation of Tyr716. At known biological EC50 doses, inhibition of Erk5 and JNK was ~60% and ~35% effective against proliferation of A172 and T98G. When all four MAPK families were inhibited, a complete block of proliferation occurred in both cell lines, similarly to the case where the initial activation step of Raf by Ras was inhibited.

3.5. Activation of the Akt survival kinase shows similar patterns in sparse and confluent cultures

Western blotting also confirmed that ligand stimulation induced phosphorylation of Tyr751 residues under both sparse and confluent growth conditions (Fig. 5A). Tyr751 phosphorylation feeding into the PI3K pathway started within a minute of stimulation, decayed almost to background after an hour, and was somewhat higher in sparse cultures than in confluent ones. However, Akt phosphorylation did not show marked corresponding differences, possibly because of the multiplicity of various inputs targeting the Akt pathway. Consequently, we observed no significant tendentious differences in the spontaneous apoptotic rate and in heat-shock induced apoptosis of sparse versus confluent cells (data not shown).

3.6. Activation of the PLC γ pathway and consequential cell migration is dominant in confluent cultures

Phosphorylation of Tyr1021 occurred both in sparse and confluent cells, started by the first minute of stimulation, but was over within half an hour. Confluent cells showed markedly higher p-Tyr1021 than sparse cells of both cell lines. The phosphorylation of RhoA, an important effector activated along the PLC γ /PKC pathway, was correspondingly also greatly increased in confluent cells, while in sparse cells it remained at baseline with only a slight increase at 2–15 min. Immunofluorescence images in Fig. 5B (top row) also show that 2 h after stimulation RhoA phosphorylation can even be below the baseline seen in unstimulated cells, while in confluent cells it is still maintained at a very high level.

Based on this observation, we hypothesized that activation of the PLC γ pathway in confluent cells has a functional consequence on cell migration. Cortactin is an important protein facilitating polymerization and rearrangement of the actin cytoskeleton, promoting the formation of lamellipodia, invadopodia, and cell migration. Fig. 5B shows that cellular localization and rearrangement of this protein to the leading edges were oppositely regulated in sparse and confluent cultures. In resting sparse cells, cortactin was mostly localized to the polarized cell front protrusion but decreased in quantity and appeared perinuclearly 2 h after stimulus. In unstimulated confluent cultures, cortactin dominantly showed cytoplasmic localization, but following PDGF-BB stimulation, it cumulated in the polarized leading cell front.

For a functional assay, next we directly monitored and quantitatively analyzed cell motility using live cell microscopy and tracking. This assay complies well with our model where no chemotactic gradient is implied, yet migration rate of cells increases with their local density. Fig. 6A shows the tracks of observed cells centered to start at coordinates (0,0), with tracks of sparse cells (in red) overlaid the tracks of confluent cells (in black). Owing to tracks ending with the mitotic event at various time points, cumulated tracks are plotted for 200, 500 and 1500 min observation time to give a broader picture of migratory tendencies for both A172 and T98G cells. It is very clear that confluent cultures of both cell lines show increased migration at all time points. Accumulated distance (Fig. 6B) and Euclidean distance (absolute displacement, Fig. 6C) were plotted as a function of cumulative observation time in 100 min steps. As expected from the cell tracks, confluent cultures of both cell lines covered at least twice longer distances over the same time, got at least twice further from their starting point. Since with time more and more cell tracks ended due to mitosis, both these plots flatten to a plateau. The sparse cultures reach the plateau

sooner; the linear phase for confluent cells is longer, coherent with divisions occurring sooner on average in sparse cultures. Average velocity was also higher in confluent cultures, and did not change over time; therefore only the overall averages were plotted (Fig. 6D).

4. Discussion

Earlier we have observed that PDGF stimulated glioblastoma cells respond with a two-phase calcium signal constituted of intracellular release followed by sustained influx from the extracellular space [28,33]. Interestingly, as opposed to confluent cells, those in sparse cultures mostly displayed a reduced response; shorter, lower spikes, or no transients at all [27]. It has also been known for long [24] that normal cells undergo contact inhibition, while malignant transformation often abrogates this regulatory feature of mammalian cells. While there are various proposed mechanisms of contact inhibition [34–36], the idea of a confluence dependent regulatory mechanism immediately at the first branching level of the input signal through receptor tyrosine kinases seemed compelling. In fact, we have observed that a differential phosphorylation of several tyrosine residues of PDGFR- β receptors was evoked by PDGF stimulation in glioblastoma cells as a function of cell confluence.

This differential phosphorylation took place primarily in GM1-rich lipid rafts, regardless of the residue concerned, which is coherent with the ample evidence cumulated in the literature that lipid rafts serve as organizing platforms for growth factor receptors [19,21,23,37]. While there was a gradual increase of receptor expression with cell confluence (data not shown), and a parallel increase of the raft-localization of these receptors, even in the sparse state, more phosphorylated tyrosine residues were found in lipid rafts, as evidenced by our microscopic pixel-by-pixel quantitation algorithm. The major difference was the identity of the residue. Some of the examined residues were predominantly activated in sparse cells, yet others in confluent ones.

In sparse cultures, both absolute and relative phosphorylation of tyrosine 716 specific to the Ras/MAPK pathway and tyrosine 751 specific to the PI3-kinase/Akt pathway [10] were increased upon ligand stimulation, dominantly in GM1 rich clusters of the cell membrane. On the other hand, in confluent cultures, tyrosine 771 that serve as an adaptor for Ras-GAP inactivating the MAPK pathway [12], and tyrosine 1021 feeding into the PLC γ /PKC pathway [16] were the ones that showed significant phosphorylation. These findings in single cell microscopy were confirmed for cell populations by Western blotting.

Western blotting was then also used to verify that consecutive downstream steps in signaling are coherent with the differential phosphorylation of tyrosine residues. As logically expected, phosphorylated p38-MAPK, and also p42/44-MAPK were increased in sparse cultures upon PDGF stimulus, in coherence with increased Tyr716 phosphorylation. Meanwhile, in confluent cells, MAPK phosphorylation was low, partly owed to the lower levels of p-Tyr716, and partly to the strong phosphorylation of Tyr771, which inhibits the MAPK pathway by activating Ras-GAP. In confluent cells, increased phosphorylation of Tyr1021 not only yielded a two-phase calcium signal as observed formerly [27], but also enhanced RhoA phosphorylation likely as a result of PKC activation [38]. Regarding Akt phosphorylation, we have not seen major differences between confluent and sparse cells, which is probably the result of the very many diverse inputs that lead to Akt phosphorylation and pro-survival signaling, and is also a reasonable finding considering that both migrating and proliferating tumor cells need antiapoptotic signals.

As a proof of concept, at the molecular level we have looked at functional-morphological markers of proliferation and migration: Ki-67 with nuclear localization and cortactin in the leading edge. The majority of sparse cells stimulated with PDGF exhibited a high level of nuclear Ki-67 immunoreactivity, coherent with the activated proliferation pathways. At the same time, in confluent cells, nuclear Ki-67 signal was hardly visible. However, these cells showed marked pRhoA

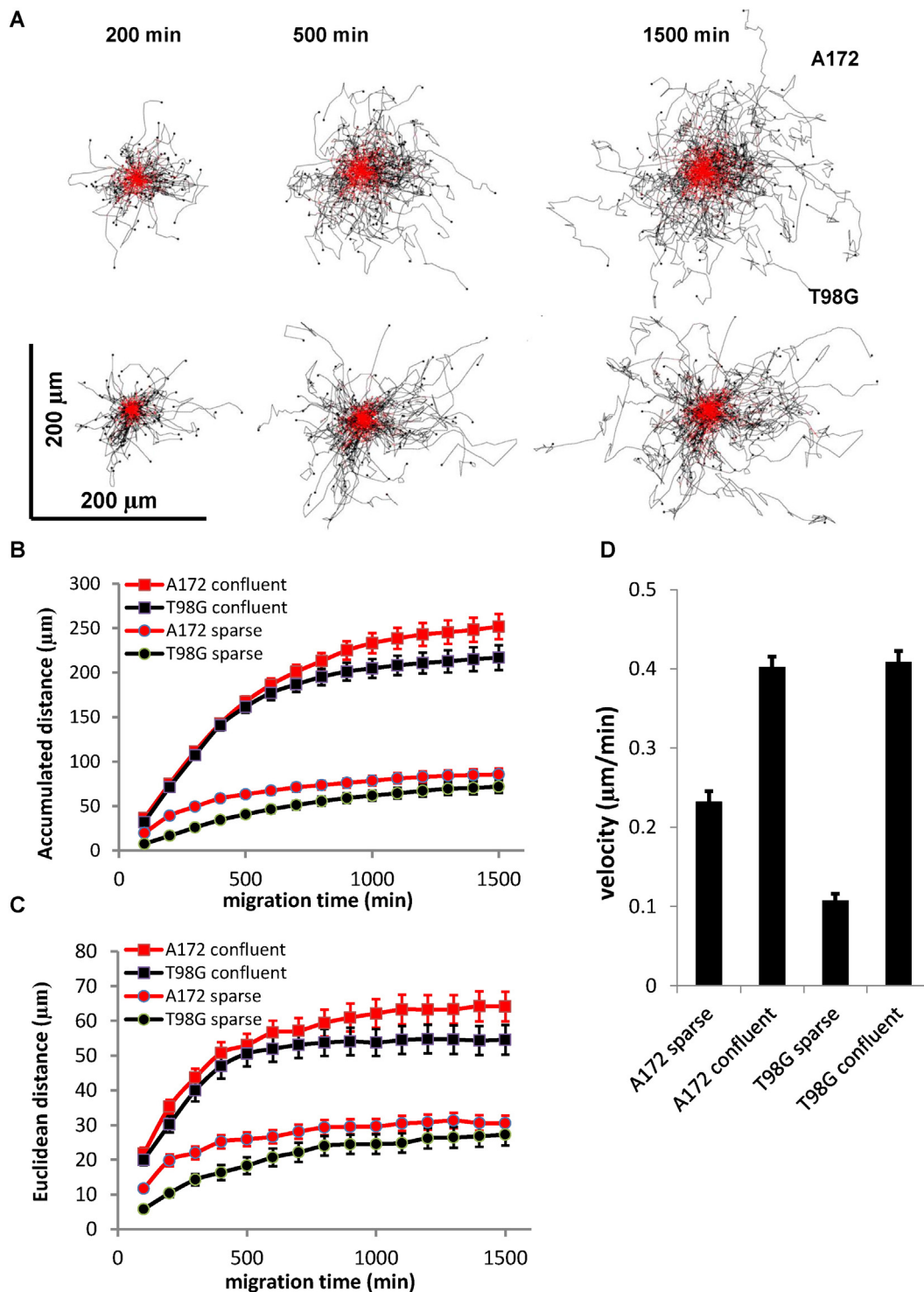


Fig. 6. Live cell imaging as functional proof of increased motility in confluent cultures. Cells seeded at 8000 and 32,000 per well were stimulated with 2 ng/ml PDGF-BB and imaged after adhesion and spreading for minimum 36 h taking one frame at every 10 min and tracked until their first division. A: Tracks of A172 and T98G cells at various cumulative time points. Graphs representing all (≥ 100) cell tracks centered to start at coordinates (0,0) were plotted for 200, 500 and 1500 min observation time. Tracks of sparse cells (in red) were overlaid the tracks of confluent cells (in black). B: Accumulated migration distance as a function of accumulation time. Accumulated distance was plotted as a function of accumulation time, increased in 100 min steps. A172 cells are represented with black plots, T98G with red, confluent cells are shown with squares, sparse ones with circles. Data are mean of ≥ 100 cells \pm SEM from three experiments. C: Euclidean distance as a function of accumulation time. Euclidean distance (absolute displacement from the starting point) was plotted as a function of accumulation time, increased in 100 min steps. A172 cells are represented with black plots, T98G with red, confluent cells are shown with squares, sparse ones with circles. Data are mean of ≥ 100 cells \pm SEM from three experiments. D: Migration velocity in sparse and confluent cultures. Migration velocity is plotted as a function cell type and confluence. Data are mean of ≥ 100 cells \pm SEM from three experiments. (For interpretation of the references to color in this figure legend, the reader is referred to the web version of this article.)

630 immunoreactivity also in fluorescence microscopy, paralleled with an
631 accented cortactin signal in leading edges. On the contrary, sparse
632 cells have lost even those cortactin-rich protrusions upon stimulus
633 that were visible at rest.

To verify the altered cellular functions, the proliferation rates and
634 motilities of sparse and confluent cultures have been compared. As re-
635 vealed by metabolic and real time cell adhesion assays, sparse cells pro-
636 liferated at greater rate than confluent ones; for these latter, live cell
637

imaging confirmed that the first mitotic events occurred later. Specific inhibitors of members of the MAP kinase family revealed that to some extent Erk5 and JNK are also involved in the proliferative response and that while A172 cells heavily rely on p38 MAPK in this aspect, T98G cells need to have all MAPK families inhibited for a complete proliferation block. As expected, inhibition of the MAPK pathway at its input of Ras/Raf interaction totally abolished proliferation in both cell lines. Live cell imaging also revealed that migration velocity and total accumulated distance were greater in confluent cultures by a factor of 2 and 4 for A172 and T98G, and total displacement was greater by a factor >2 for both. Overall, the final cellular responses observed were coherent with the initial differential phosphorylation of the PDGF receptor β .

Such differential phosphorylation is not likely to be implemented directly during receptor activation and transphosphorylation, rather, one possible explanation is the active, and confluence dependent participation of phosphatases. Regulation of PDGFR by phosphotyrosine-phosphatases is known in quite some detail [39–41]. Based on these investigations, PTPN1, PTPN4, and PTPN11 [42,43] are the best candidates for differentially dephosphorylating the tyrosine residues of activated receptors. It remains to be seen whether these are regulated by cell confluence at the level of expression, activity, or raft/non-raft redistribution.

5. Conclusions

Cumulatively, our observations suggest that the same stimulus is able to promote distinct signaling outputs through a regulatory mechanism driven by cell confluence and based on segregation in lipid rafts. These altered outputs are highly relevant for tumor proliferation and spreading. Specifically, cell division dominates in sparse cultures and promotion of migration is accompanied by a mitigated proliferative response in confluent monolayers showing contact inhibition. This mechanism could be a genuine strategy of tumor cells to use the same signaling machinery for providing responses optimized for their environmental circumstances, and is not restricted to a single cell line, as both A172 and T98G behaved in a similar manner, with minor differences only in the time-course of activation processes and the spectrum of relevant MAPK kinases. On the other hand, non-malignant primary fibroblasts, such as the AG01523B, expressing the same PDGFR- β in their membrane, do not show responses optimized for continuous proliferation and spreading, contact inhibited cells do not start to migrate (data not shown).

From the pathological perspective, our experiments reveal the differential phosphorylation of important tyrosine residues on the PDGF receptor tyrosine kinase in the membrane of confluent and sparse cells, in spite of both types of cells encountering the very same PDGF-BB stimulus. The differentially phosphorylated residues activate their respective relevant downstream pathways, which evoke, depending on the state of cell confluence, a cellular response which is very logical from the point of view of an invasive tumor. Densely packed cells modeling the lack of space in locally growing tumors respond to stimulus by migration, an important step on the route to invasion or metastasis, while sparse cells, modeling freshly settled disseminated tumor cells respond to the same stimulus by vigorous proliferation.

Declaration of conflict of interests

None of the authors have conflicts interest.

Acknowledgments

We acknowledge the financial support from the Hungarian Scientific Research Fund (OTKA K75752, NK 101337), and the Baross Gabor Program (REG-EA-09-1-2009-0010). We wish to thank Eszter Molnár and Tamás Garay at the 2nd Dept. of Pathology, Semmelweis University,

Budapest, Hungary, for running a pilot experiment on cell migration. We also are grateful to József Tóvári (Department of Experimental Pharmacology, National Institute of Oncology, Budapest, Hungary) for valuable discussion on cell migration.

References

- C.H. Heldin, B. Westermark, Mechanism of action and in vivo role of platelet-derived growth factor, *Physiol. Rev.* 79 (1999) 1283–1316.
- H. Ren, B.F. Yang, N.G. Rainov, Receptor tyrosine kinases as therapeutic targets in malignant glioma, *Rev. Recent Clin. Trials* 2 (2007) 87–101.
- M. Nister, L. Claesson-Welsh, A. Eriksson, C.H. Heldin, B. Westermark, Differential expression of platelet-derived growth factor receptors in human malignant glioma cell lines, *J. Biol. Chem.* 266 (1991) 16755–16763.
- D. Smith, T. Shimamura, S. Barbera, B.E. Bejcek, NF-kappaB controls growth of glioblastomas/astrocytomas, *Mol. Cell. Biochem.* 307 (2008) 141–147.
- T.B. Mapstone, Expression of platelet-derived growth factor and transforming growth factor and their correlation with cellular morphology in glial tumors, *J. Neurosurg.* 75 (1991) 447–451.
- A.H. Shih, C. Dai, X. Hu, M.K. Rosenblum, J.A. Koutcher, E.C. Holland, Dose-dependent effects of platelet-derived growth factor-B on glial tumorigenesis, *Cancer Res.* 64 (2004) 4783–4789.
- K. Majumdar, B.D. Radotra, R.K. Vasishtha, A. Pathak, Platelet-derived growth factor expression correlates with tumor grade and proliferative activity in human oligodendrogliomas, *Surg. Neurol.* 72 (2009) 54–60.
- S. Camorani, C.L. Esposito, A. Rienzo, S. Catuogno, M. Iaboni, G. Condorelli, V. de Franciscis, L. Cerchia, Inhibition of receptor signaling and of glioblastoma-derived tumor growth by a novel PDGFRbeta aptamer, *Mol. Ther.* 22 (2014) 828–841.
- A.K. Arvidsson, E. Rupp, E. Nanberg, J. Downward, L. Ronnstrand, S. Wennstrom, J. Schlessinger, C.H. Heldin, L. Claesson-Welsh, Tyr-716 in the platelet-derived growth factor beta-receptor kinase insert is involved in GRB2 binding and Ras activation, *Mol. Cell. Biol.* 14 (1994) 6715–6726.
- B. Venkatesan, N. Ghosh-Choudhury, F. Das, L. Mahaimanathan, A. Kamat, B.S. Kasinath, H.E. Abboud, G.G. Choudhury, Resveratrol inhibits PDGF receptor mitogenic signaling in mesangial cells: role of PTP1B, *FASEB J.* 22 (2008) 3469–3482.
- A. Kashishian, A. Kazlauskas, J.A. Cooper, Phosphorylation sites in the PDGF receptor with different specificities for binding GAP and PI3 kinase in vivo, *EMBO J.* 11 (1992) 1373–1382.
- S. Ekman, A. Kallin, U. Engstrom, C.H. Heldin, L. Ronnstrand, SHP-2 is involved in heterodimer specific loss of phosphorylation of Tyr771 in the PDGF beta-receptor, *Oncogene* 21 (2002) 1870–1875.
- S.A. Courtneidge, R.M. Kypta, J.A. Cooper, A. Kazlauskas, Platelet-derived growth factor receptor sequences important for binding of src family tyrosine kinases, *Cell Growth Differ.* 2 (1991) 483–486.
- M. Valius, A. Kazlauskas, Phospholipase C-gamma 1 and phosphatidylinositol 3 kinase are the downstream mediators of the PDGF receptor's mitogenic signal, *Cell* 73 (1993) 321–334.
- S.R. Datta, A. Brunet, M.E. Greenberg, Cellular survival: a play in three Akts, *Genes Dev.* 13 (1999) 2905–2927.
- V. Kundra, J.A. Escobedo, A. Kazlauskas, H.K. Kim, S.G. Rhee, L.T. Williams, B.R. Zetter, Regulation of chemotaxis by the platelet-derived growth factor receptor-beta, *Nature* 367 (1994) 474–476.
- S.G. Rhee, Regulation of phosphoinositide-specific phospholipase C, *Annu. Rev. Biochem.* 70 (2001) 281–312.
- A.L. Reddi, G. Ying, L. Duan, G. Chen, M. Dimri, P. Douillard, B.J. Druker, M. Naramura, V. Band, H. Band, Binding of Cbl to a phospholipase Cgamma1-docking site on platelet-derived growth factor receptor beta provides a dual mechanism of negative regulation, *J. Biol. Chem.* 282 (2007) 29336–29347.
- P. Nagy, G. Vereb, Z. Sebestyen, G. Horvath, S.J. Lockett, S. Damjanovich, J.W. Park, T.M. Jovin, J. Szollosi, Lipid rafts and the local density of ErbB proteins influence the biological role of homo- and heteroassociations of ErbB2, *J. Cell Sci.* 115 (2002) 4251–4262.
- L.J. Pike, Growth factor receptors, lipid rafts and caveolae: an evolving story, *Biochim. Biophys. Acta* 2005 (1746) 260–273.
- G. Vereb, J. Szollosi, J. Matko, P. Nagy, T. Farkas, L. Vigh, L. Matyus, T.A. Waldmann, S. Damjanovich, Dynamic, yet structured: the cell membrane three decades after the singer-nicolson model, *Proc. Natl. Acad. Sci. U. S. A.* 100 (2003) 8053–8058.
- T. Harder, K. Simons, Clusters of glycolipid and glycosylphosphatidylinositol-anchored proteins in lymphoid cells: accumulation of actin regulated by local tyrosine phosphorylation, *Eur. J. Immunol.* 29 (1999) 556–562.
- G. Vereb, J. Matko, G. Vamosi, S.M. Ibrahim, E. Magyar, S. Varga, J. Szollosi, A. Jenei, R. Gaspar Jr., T.A. Waldmann, S. Damjanovich, Cholesterol-dependent clustering of IL-2Ralpha and its colocalization with HLA and CD48 on T lymphoma cells suggest their functional association with lipid rafts, *Proc. Natl. Acad. Sci. U. S. A.* 97 (2000) 6013–6018.
- H.W. Fisher, J. Yeh, Contact inhibition in colony formation, *Science* 155 (1967) 581–582.
- J.P. Thiery, Epithelial-mesenchymal transitions in tumour progression, *Nat. Rev. Cancer* 2 (2002) 442–454.
- T. Fiaschi, P. Chiarugi, F. Buricchi, E. Giannoni, M.L. Taddei, D. Talini, G. Cozzi, S. Zecchi-Orlandini, G. Raugi, G. Ramponi, Low molecular weight protein-tyrosine phosphatase is involved in growth inhibition during cell differentiation, *J. Biol. Chem.* 276 (2001) 49156–49163.

- 780 [27] G. Vereb, B.G. Feuerstein, W.C. Hyun, M.J. Fulwyler, M. Balazs, J. Szollosi, Biphasic
781 calcium response of platelet-derived growth factor stimulated glioblastoma cells is
782 a function of cell confluence, *Cytometry A* 67 (2005) 172–179.
- 783 [28] J. Szollosi, B.G. Feuerstein, G. Vereb, H.A. Pershadsingh, L.J. Marton, Calcium channels
784 in PDGF-stimulated A172 cells open after intracellular calcium release and are not
785 voltage-dependent, *Cell Calcium* 12 (1991) 477–491.
- 786 [29] W.S. Rasband, ImageJ, U S National Institutes of Health, Bethesda, Maryland, USA,
787 1997–2014.
- 788 [30] E. Meijering, O. Dzyubachyk, I. Smal, Methods for cell and particle tracking, *Methods*
789 *Enzymol.* 504 (2012) 183–200.
- 790 [31] T. Garay, E. Juhasz, E. Molnar, M. Eisenbauer, A. Czirok, B. Dekan, V. Laszlo, M.A.
791 Hoda, B. Dome, J. Timar, et al., Cell migration or cytokinesis and proliferation?
792 –revisiting the “go or grow” hypothesis in cancer cells in vitro, *Exp. Cell Res.* 319
793 (2013) 3094–3103.
- 794 [32] J. Tovari, K. Futosi, A. Bartal, E. Tatrai, A. Gacs, I. Kenessey, S. Paku, Boyden chamber-
795 based method for characterizing the distribution of adhesions and cytoskeletal
796 structure in HT1080 fibrosarcoma cells, *Cell Adhes. Migr.* 8 (2014) 509–516.
- 797 [33] G. Vereb Jr., J. Szollosi, L. Matyus, M. Balazs, W.C. Hyun, B.G. Feuerstein, Depletion of
798 intracellular calcium stores facilitates the influx of extracellular calcium in platelet
799 derived growth factor stimulated A172 glioblastoma cells, *Cytometry* 24 (1996)
800 64–73.
- 801 [34] Y. Takai, J. Miyoshi, W. Ikeda, H. Ogita, Nectins and nectin-like molecules: roles in
802 contact inhibition of cell movement and proliferation, *Nat. Rev. Mol. Cell Biol.* 9
803 (2008) 603–615.
- 804 [35] R.J. Wieser, S. Schutz, G. Tschank, H. Thomas, H.P. Dienes, F. Oesch, Isolation and
805 characterization of a 60–70-kD plasma membrane glycoprotein involved in the
806 contact-dependent inhibition of growth, *J. Cell Biol.* 111 (1990) 2681–2692.
- 807 [36] M.C. Moh, S. Shen, The roles of cell adhesion molecules in tumor suppression and
808 cell migration: a new paradox, *Cell Adhes. Migr.* 3 (2009) 334–336.
- 809 [37] A. de Laurentiis, L. Donovan, A. Arcaro, Lipid rafts and caveolae in signaling by
810 growth factor receptors, *Open Biochem. J.* 1 (2007) 12–32.
- 811 [38] T. Su, S. Straight, L. Bao, X. Xie, C.L. Lehner, G.S. Cavey, T.N. Teknos, Q. Pan, PKC
812 epsilon phosphorylates and mediates the cell membrane localization of RhoA,
813 *ISRN Oncol.* 2013 (2013) 329063.
- 814 [39] M. Kovalenko, K. Denner, J. Sandstrom, C. Persson, S. Gross, E. Jandt, R. Vilella, F.
815 Bohmer, A. Ostman, Site-selective dephosphorylation of the platelet-derived growth
816 factor beta-receptor by the receptor-like protein-tyrosine phosphatase DEP-1, *J.*
817 *Biol. Chem.* 275 (2000) 16219–16226.
- 818 [40] B. Markova, P. Herrlich, L. Ronnstrand, F.D. Bohmer, Identification of protein tyrosine
819 phosphatases associating with the PDGF receptor, *Biochemistry* 42 (2003)
820 2691–2699.
- 821 [41] C. Persson, C. Savenhed, A. Bourdeau, M.L. Tremblay, B. Markova, F.D. Bohmer, F.G.
822 Haj, B.G. Neel, A. Elson, C.H. Heldin, et al., Site-selective regulation of platelet-
823 derived growth factor beta receptor tyrosine phosphorylation by T-cell protein
824 tyrosine phosphatase, *Mol. Cell. Biol.* 24 (2004) 2190–2201.
- 825 [42] M. Dagnell, J. Frijhoff, I. Pader, M. Augsten, B. Boivin, J. Xu, P.K. Mandal, N.K. Tonks, C.
826 Hellberg, M. Conrad, et al., Selective activation of oxidized PTP1B by the thioredoxin
827 system modulates PDGF-beta receptor tyrosine kinase signaling, *Proc. Natl. Acad.*
828 *Sci. U. S. A.* 110 (2013) 13398–13403.
- 829 [43] J.H. Wu, R. Goswami, X. Cai, S.T. Exum, X. Huang, L. Zhang, L. Brian, R.T. Premont, K.
830 Peppel, N.J. Freedman, Regulation of the platelet-derived growth factor receptor-
831 beta by G protein-coupled receptor kinase-5 in vascular smooth muscle cells
832 involves the phosphatase Shp2, *J. Biol. Chem.* 281 (2006) 37758–37772.